MUSTA schemes for multi-dimensional hyperbolic systems: analysis and improvements

V.A. Titarev[1] and E.F. Toro[2]

[1] Department of Mathematics, Faculty of Science,
University of Trento, Trento, Italy,
E-mail: titarev@science.unitn.it,
Web page: http://www.science.unitn.it/∼titarev

[2] Laboratory of Applied Mathematics, Faculty of Engineering,
University of Trento, Trento, Italy,
E-mail: toro@ing.unitn.it,
Web page: http://www.ing.unitn.it/toro

We develop and analyze an improved version of the Multi-Stage (MUSTA) approach to the construction of upwind Godunov-type fluxes whereby the solution of the Riemann problem, approximate or exact, is not required. The new MUSTA schemes improve upon the original schemes in terms of monotonicity properties, accuracy and stability in multiple space dimensions. We incorporate the MUSTA technology into the framework of finite-volume weighted essentially non-oscillatory schemes as applied to the Euler equations of compressible gas dynamics. The results demonstrate that our new schemes are good alternatives to current centred methods and to conventional upwind methods as applied to complicated hyperbolic systems for which the solution of the Riemann problem is costly or unknown.

Key words: MUSTA flux, Riemann solver, FORCE flux, stability in multiple space dimensions, weighted essentially non-oscillatory.

1 Introduction

Godunov-type upwind finite-volume methods represent a popular class of modern numerical tools for solving hyperbolic systems of conservation laws. The key idea behind the original first-order scheme [3] is to incorporate into the numerical flux the physics of wave propagation via the self-similar solution of the local Riemann problem. Higher-order versions can be constructed by using piece-wise polynomial representation of data [5, 20, 2, 11]. The resulting high-order upwind schemes are accurate, reliable and applicable to a large variety of systems of conservation laws. See [14, 7] for recent reviews on Godunov-type methods for equations of compressible gas dynamics, magnetohydrodynamics and elasticity.

An alternative to the upwind methods is represented by the class of so-called centred, or symmetric, methods [8, 9, 13]. The construction of corresponding centred numerical fluxes does not require a detailed knowledge of the structure of the Riemann problem solution. This makes them simple and efficient but also quite diffusive as compared to the Godunov-type fluxes. The truncation error of the centred schemes is inversely proportional to the Courant number coefficient resulting in very poor resolution of slowly moving waves, especially those associated with linearly degenerate fields, such as contact waves, shear waves and vortices. Additionally, the known first-order centred fluxes are not directly applicable to the construction of multidimensional unsplit schemes because resulting finite-volume methods are unconditionally unstable [17]. Development of stable multidimensional centred schemes requires the use of special predictor-corrector techniques, leading to additional and quite substantial complexity, see [18, 10] and references therein.

A recent approach for the construction of numerical fluxes that combine good properties of upwind fluxes and simplicity of centred fluxes is the Multi-Stage (MUSTA) approach [15, 16]. The key idea behind MUSTA is to solve the local Riemann problem numerically rather than analytically by means of a simple and computationally inexpensive first-order centred method. By using local time marching one effectively resolves the correct structure of the solution of the local Riemann problem and then uses this information for evaluating the numerical flux. The resulting upwind MUSTA schemes are found to be considerably more accurate than the centred methods and comparable to upwind methods [15, 16]. Additionally, the unsplit finite-volume MUSTA schemes are stable in multiple space dimensions which allows one to use the corresponding MUSTA fluxes in the construction of higher-order Godunov-type methods [16, 12].

Despite significant improvements over centred methods in terms of accuracy and stability in multiple space dimensions, offered by the MUSTA approach, one important problem

remains: the truncation error of the scheme is still inversely proportional to the Courant number coefficient. This means that the performance of the scheme will be inferior to that of good upwind methods when a small Courant number needs to be used. We note, however, that the coefficient of the leading term of the truncation error of MUSTA schemes is several times smaller than that of centred methods, and thus the impact on accuracy will also be smaller.

The aim of this paper is twofold. Firstly, we analyze in detail the properties of the original MUSTA approach [15, 16], such as consistency and stability in multiple space dimensions. Secondly, we develop an improved version of MUSTA which is obtained from the original MUSTA by changes in the local time stepping procedure. The improvements are threefold. Firstly, the new MUSTA flux converges to the Godunov flux as the number of stages grows and therefore, the resulting flux is monotone. Secondly, the truncation error of the new MUSTA schemes is a linear function of the Courant number coefficient and does not depend on the reciprocal of the Courant number coefficient. Thirdly, the stability region of the new MUSTA scheme coincides with that of the Godunov method and is larger than that of the original variant.

We provide numerical examples for the compressible Euler equations in one, two and three space dimensions. These examples demonstrate that the new MUSTA schemes effectively match the accuracy of the Godunov method with state-of-the art Riemann solvers. We also show the ease with which it is possible to incorporate the developed MUSTA flux into existing finite-volume schemes.

The rest of the paper is organized as follows. In Section 2 we outline the general framework of multidimensional finite-volume schemes. In Section 3 we describe the original and improved MUSTA schemes. In Section 4 we study the properties of the schemes in one space dimension. In Section 5 we analyze the stability of the MUSTA schemes in multiple space dimensions. Remarks on the practical implementation for nonlinear systems are given in Section 6. Numerical results are provided in Section 7 and conclusions are drawn in Section 8.

2 Finite-volume schemes in multiple space dimensions

Consider three-dimensional hyperbolic systems in conservation form

$$\partial_t \mathbf{Q} + \partial_x \mathbf{F}(\mathbf{Q}) + \partial_y \mathbf{G}(\mathbf{Q}) + \partial_z \mathbf{H}(\mathbf{Q}) = \mathbf{0}, \tag{1}$$

where $\mathbf{Q}(x, y, z, t)$ is the vector of unknown conservative variables and $\mathbf{F}(\mathbf{Q})$, $\mathbf{G}(\mathbf{Q})$ and $\mathbf{H}(\mathbf{Q})$ are physical flux vectors in x, y and z coordinate directions respectively. Integrat-

ing (1) over a control volume (a computational cell) in $x-y-z$ space of dimensions $\Delta x = x_{i+\frac{1}{2}} - x_{i-\frac{1}{2}}$, $\Delta y = y_{j+\frac{1}{2}} - y_{j-\frac{1}{2}}$, $\Delta z = z_{k+\frac{1}{2}} - z_{k-\frac{1}{2}}$, we obtain the following semi-discrete relation

$$\begin{aligned}\frac{d}{dt}\mathbf{Q}_{ijk}(t) = \quad & \frac{1}{\Delta x}\left(\mathbf{F}_{i-1/2,jk} - \mathbf{F}_{i+1/2,jk}\right) + \frac{1}{\Delta y}\left(\mathbf{G}_{i,j-1/2,k} - \mathbf{G}_{i,j+1/2,k}\right) + \\ & \frac{1}{\Delta z}\left(\mathbf{H}_{ij,k-1/2} - \mathbf{H}_{ij,k+1/2}\right),\end{aligned} \tag{2}$$

where, as usual, $\mathbf{Q}_{ijk}(t)$ is the spatial average of the solution in the cell at time t and $\mathbf{F}_{i+1/2,jk}$, $\mathbf{G}_{i,j+1/2,k}$ and $\mathbf{H}_{ij,k+1/2}$ are spatial averages of physical fluxes over cell faces at time t. The simplest scheme which can be considered from the above framework results from assuming initial data at time t^n as given by a set of piece-wise constant values $\mathbf{Q}_{ijk}$ and using the Euler time-stepping to discretize the time derivative to obtain

$$\begin{aligned}\mathbf{Q}_{ijk}^{n+1} = \mathbf{Q}_{ijk}^{n} + \quad & \frac{\Delta t}{\Delta x}\left(\mathbf{F}_{i-1/2,jk} - \mathbf{F}_{i+1/2,jk}\right) + \frac{\Delta t}{\Delta y}\left(\mathbf{G}_{i,j-1/2,k} - \mathbf{G}_{i,j+1/2,k}\right) + \\ & \frac{\Delta t}{\Delta z}\left(\mathbf{H}_{ij,k-1/2} - \mathbf{H}_{ij,k+1/2}\right).\end{aligned} \tag{3}$$

The description of the scheme (3) is complete once expressions for the numerical fluxes are provided. Godunov [3] proposed to use the self-similar solution $\mathbf{Q}_*(x/t)$ of the local Riemann problem to compute numerical fluxes in the direction normal to the cell faces. For example, for $\mathbf{F}_{i+1/2}$ the local Riemann problem is given by

$$\frac{\partial}{\partial t}\mathbf{Q} + \frac{\partial}{\partial x}\mathbf{F} = \mathbf{0}, \quad \mathbf{Q}(x,0) = \begin{cases} \mathbf{Q}_L = \mathbf{Q}_{ijk}, & x < 0, \\ \mathbf{Q}_R = \mathbf{Q}_{i+1,jk}, & x > 0. \end{cases} \tag{4}$$

The original Godunov flux is given by $\mathbf{F}_{i+1/2} = \mathbf{F}(\mathbf{Q}_*(0))$. More generally, the numerical flux can be defined as a two-point function of left and right data in the local Riemann problem:

$$\mathbf{F}_{i+1/2} = \mathbf{F}_{i+1/2}(\mathbf{Q}_L, \mathbf{Q}_R). \tag{5}$$

In most cases the upwind Godunov-type fluxes cannot be written as an explicit function of $\mathbf{Q}_L$, $\mathbf{Q}_R$. Centred fluxes can be written in the form (5), which makes them simple to implement and applicable to a wider class of the hyperbolic systems. However, they cannot be directly used in (3) since the resulting finite-volume scheme is unconditionally unstable [17].

Higher-order extensions of the basic scheme (3) can be constructed in a number of waves. The simplest spatially second order and monotone scheme results from using the limited piece-wise linear reconstruction of data inside each cell [5, 6]. In this paper we consider the weighted essentially non-oscillatory schemes, see [11] and references therein, in which one combines piece-wise polynomial representation of data inside each computational cell with high-order Runge-Kutta methods for time discretization. The numerical

fluxes in WENO methods are obtained by approximating the integrals of the physical flux over cell faces by a certain quadrature and then using a first-order flux, computed from (4), as a building block for each pair of boundary extrapolated values at the integration point. The only difference is that now the left and right data are not equal to cell averages but obtained by means of the WENO reconstruction procedure.

3 MUSTA numerical fluxes

A very simple and general approach to the construction of numerical fluxes, which combines the simplicity of centred fluxes and the good accuracy of the Godunov method, is the Multi-Stage (MUSTA) approach [15, 16]. The key idea of the original MUSTA is to open the Riemann fan by evolving in time the initial data $\mathbf{Q}_L$, $\mathbf{Q}_R$ in (4) via the governing equations and can be explained as follows.

Assume we know the values $\mathbf{Q}_L^{(l)}$, $\mathbf{Q}_R^{(l)}$, adjacent to the interface $x_{i+1/2}$, at the stage (local time step) l. Integrating (4) over the left $[-\Delta x, 0] \times [0, \Delta t]$ and right $[0, +\Delta x] \times [0, \Delta t]$ control volumes and using transmissive boundary conditions at $x = \pm\Delta x$ we obtain the following relations (in local coordinates)

$$\begin{aligned} \mathbf{Q}_L^{(l+1)} &= \mathbf{Q}_L^{(l)} - \frac{\Delta t}{\Delta x}\left[\mathbf{F}_{1/2}^{(l)} - \mathbf{F}_L^{(l)}\right], \quad \mathbf{F}_L^{(l)} = \mathbf{F}(\mathbf{Q}_L^{(l)}), \\ \mathbf{Q}_R^{(l+1)} &= \mathbf{Q}_R^{(l)} - \frac{\Delta t}{\Delta x}\left[\mathbf{F}_R^{(l)} - \mathbf{F}_{1/2}^{(l)}\right], \quad \mathbf{F}_R^{(l)} = \mathbf{F}(\mathbf{Q}_R^{(l)}). \end{aligned} \tag{6}$$

Here $\mathbf{F}_{1/2}^{(l)}$ is computed by using a certain monotone scheme with the evolved data at stage l:

$$\mathbf{F}_{1/2}^{(l)} = \mathbf{F}(\mathbf{Q}_L^{(l)}, \mathbf{Q}_R^{(l)}). \tag{7}$$

From the point of view of simplicity and efficiency a first-order monotone centred scheme is the best choice. Here we use the First-Order Centred Scheme (FORCE) [13]. The corresponding flux of the form (5) is given by the following expression:

$$\begin{aligned} \mathbf{F}^{FORCE}(\mathbf{Q}_L, \mathbf{Q}_R) &= \frac{1}{4}\left(\mathbf{F}_L + 2\mathbf{F}_M + \mathbf{F}_R - \frac{\Delta x}{\Delta t}(\mathbf{Q}_R - \mathbf{Q}_L)\right), \\ \mathbf{F}_M &= \mathbf{F}\left(\mathbf{Q}^{1/2}\right), \quad \mathbf{Q}^{1/2} = \frac{1}{2}\left(\mathbf{Q}_L + \mathbf{Q}_R) - \frac{\Delta t}{\Delta x}(\mathbf{F}_R - \mathbf{F}_L)\right). \end{aligned} \tag{8}$$

For discussion on properties of the FORCE scheme, including convergence for two-by-two nonlinear hyperbolic systems, see [14, 1].

The procedure to evaluate the MUSTA flux as given in [15, 16] can now be summarized as follows. The multi-staging (or local time stepping) is started by setting $\mathbf{Q}_L^{(0)} \equiv \mathbf{Q}_L$, $\mathbf{Q}_R^{(0)} \equiv \mathbf{Q}_R$ for the initial stage $l = 0$. Then for $0 \le l \le L - 1$, where L is the desired number of stages, we do

1. Compute the FORCE flux (8) on data at the stage l as $\mathbf{F}^{(l)}_{1/2} = \mathbf{F}^{FORCE}(\mathbf{Q}^{(l)}_L, \mathbf{Q}^{(l)}_R)$
2. Update the left and right data using (6).
3. Goto to step 1

Note that the global time step Δt from the simultaneous update (3) is used in the local time marching (6) and FORCE flux (8). The final MUSTA flux is given by $\mathbf{F}^{MUSTA}_{i+1/2} = \mathbf{F}^{(L)}_{1/2} = \mathbf{F}^{FORCE}(\mathbf{Q}^{(L)}_L, \mathbf{Q}^{(L)}_R)$. We also remark that the case $L = 0$ reproduces the FORCE scheme.

An improved version of the above flux can be constructed by using a larger local computational domain and choosing the time step in the local time marching (6) from the local data. Effectively, this is equivalent to solving the local Riemann problem (4) numerically. Let us introduce a local spatial domain and the corresponding mesh with $2M$ cells: $-M + 1 \le m \le M$. As before, the boundary between cells $m = 0$ and $m = 1$ corresponds to the interface position $x_{i+1/2}$ in (4). We again apply transmissive boundary conditions at numerical boundaries $x_{\pm M+1/2}$. The local time marching is then organized as follows:

1. Apply transmissive boundary conditions $\mathbf{Q}^{(l)}_{-M} = \mathbf{Q}^{(l)}_{-M+1}$, $\mathbf{Q}^{(l)}_{M+1} = \mathbf{Q}^{(l)}_M$
2. For $m = -M, \ldots, M$ compute the fluxes on data from stage l using the global cell size Δx (as before) and local time step Δt_{loc} in (8).
3. For $m = -M + 1, \ldots, M$ advance the local solution:

$$\mathbf{Q}^{(l+1)}_m = \mathbf{Q}^{(l)}_m - \frac{\Delta t_{loc}}{\Delta x}\left(\mathbf{F}^{(l)}_{m+1/2} - \mathbf{F}^{(l)}_{m-1/2}\right). \tag{9}$$

As before, at the end of the time marching the MUSTA flux is given by $\mathbf{F}^{MUSTA}_{i+1/2} = \mathbf{F}^{(L)}_{1/2}$. The local time step $\Delta t_{loc} = t^{l+1} - t^l$ is now calculated from the data in the local Riemann problem using the stability condition of the underlying FORCE scheme.

4 Analysis of the schemes in one space dimension

In this section we study the resulting MUSTA schemes as applied to the following model linear advection equation with constant coefficient $a \ge 0$:

$$\frac{\partial}{\partial t} q + \frac{\partial}{\partial x} f(q) = 0, \quad f = aq. \tag{10}$$

The first-order MUSTA scheme for the above equation reads

$$q^{n+1}_i = q^n_i - \frac{\Delta t}{\Delta x}\left(f_{i+1/2} - f_{i-1/2}\right),$$

where the numerical flux is given by

$$f_{i+1/2} = \beta_L \times (aq_i^n) + \beta_R \times (aq_{i+1}^n) = \beta_L \times (aq_L) + \beta_R \times (aq_R).$$

We first recall expressions for flux coefficients β_L, β_R as well as the coefficient of the leading term of the truncation error δ for some well-known first order schemes. For the Godunov scheme [3] we have

$$\beta_L = \frac{1}{2}(1 + \text{sign}(a)), \quad \beta_R = \frac{1}{2}(1 - \text{sign}(a)), \quad \delta = \frac{1}{2}a\Delta x(1 - K),$$

where K is the Courant number $K = a\Delta t/\Delta x$. For the FORCE scheme we have

$$\beta_L = \frac{(K+1)^2}{2K}, \quad \beta_R = -\frac{(1-K)^2}{2K}, \quad \delta = a\Delta x\frac{1-K^2}{4K}$$

It can be easily seen that the Godunov scheme is the optimal first order monotone scheme as applied to the model equation (10) in that it has the smallest truncation error proportional to the wave speed. The truncation error of FORCE is inversely proportional to the Courant number K and thus the numerical diffusion does not vanish as $a \to 0$. The same is true for another centred scheme, the Lax-Friedrichs scheme [8]. For small values of K we have $\delta_{FORCE} \sim a\Delta x/(4K) = \Delta x^2/(4\Delta t)$ for the FORCE scheme and $\delta_{LF} \sim a\Delta x/(2K) = \Delta x^2/(2\Delta t)$ for the Lax-Friedrichs scheme. Therefore, unlike the Godunov method, the centred schemes cannot resolve stationary discontinuities exactly.

We now proceed to analyze the MUSTA schemes. Table 1 contains expressions for flux coefficients β_L, β_R as well as the coefficient of the leading term of the truncation error δ for the original MUSTA scheme which are obtained by applying the algorithm (6) to the model equation (10). Fig. 1 shows the plots of flux coefficients as function of K for $L = 0$, 1, 3, 5. We first note that in the special case $K = 1$ the MUSTA flux reproduces the optimal Godunov flux identically and $\delta \equiv 0$. Selecting $L = 0$ results in the FORCE scheme. Next, we observe that the truncation error of MUSTA, though still inversely proportional to K, is much smaller than that of the centred schemes and for $K \sim 0$ can be written asymptotically as $\delta = 2^{-L}\,\delta_{FORCE}$.

A desirable property of a numerical flux is monotonicity. Recall that the flux is called monotone if the following conditions are satisfied:

$$\frac{\partial}{\partial q_L} f_{i+1/2} \geq 0, \quad \frac{\partial}{\partial q_R} f \leq 0.$$

It is easy to see that Godunov and FORCE fluxes are monotone for $0 \leq K \leq 1$. However, from Fig. 1 it is seen that the MUSTA fluxes of Table 1 are not monotone. Although the left coefficient $\beta_L > 0$ is always positive, the right coefficient is not negative in the full range of the Courant number K. The analysis of the case $L = 1$ is given in [15, 16],

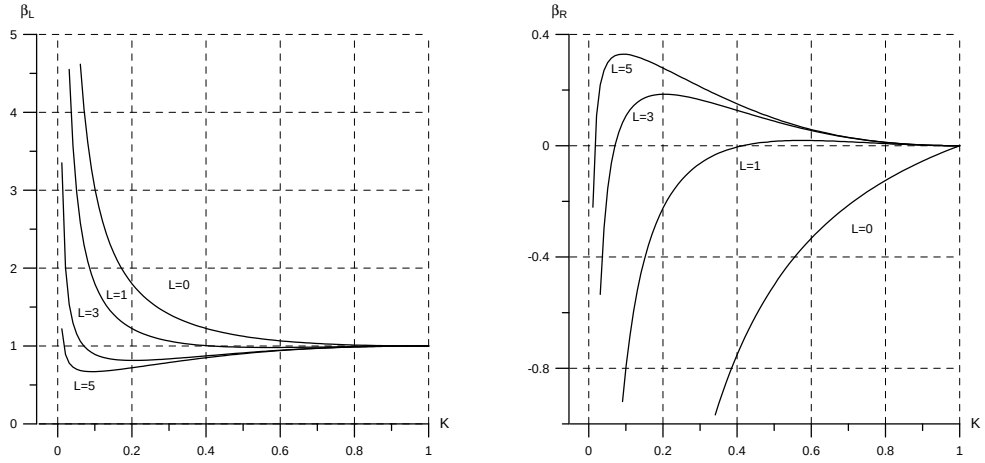

Figure 1: Plots of the flux coefficients β_L, β_R for the original MUSTA scheme (6)

where it is shown that the scheme is not monotone for $\sqrt{2}-1 < K < 1$. The maximum of β_R in this case occurs at $K \approx 0.58$ and is equal to $\beta_R \approx 0.02$. This is negligible from the practical point of view. However, as L grows, the loss of monotonicity becomes more serious due to the boundary effects in the local time stepping and manifests itself starting from smaller K as well. For $L = 3$ the maximum of β_R occurs at $K \approx 0.20$ and is equal to 0.19 whereas for $L = 10$ the maximum occurs at $K \approx 0.0157$ and is equal to 0.47.

L	β_L	β_R	$\delta/(a\Delta x)$
0	$\frac{K^2+1+2K}{4K}$	$-\frac{-2K+K^2+1}{4K}$	$-\frac{K^2-1}{4K}$
1	$-\frac{-1-4K^2-4K+K^4}{8K}$	$\frac{K^4-4K^2-1+4K}{8K}$	$-\frac{K^4-1}{8K}$
2	$\frac{-5K^4+K^6+8K+1+11K^2}{16K}$	$-\frac{K^6+1-5K^4-8K+11K^2}{16K}$	$\frac{1-5K^4+3K^2+K^6}{16K}$
3	$-\frac{K^8-26K^2-16K-6K^6+16K^4-1}{32K}$	$\frac{16K^4+K^8-26K^2+16K-6K^6-1}{32K}$	$-\frac{-10K^2+16K^4+K^8-6K^6-1}{32K}$

Table 1: Flux coefficients and the normalized coefficient of the leading term of the truncation error for the original MUSTA schemes (6).

We now proceed to analyze the improved MUSTA scheme as given by (9). We first study a special case $M > L$, in which the boundary conditions in the local time marching do not affect the local solution. The flux coefficients β_L, β_R are obtained by applying the algorithm (9) to (10) and are given in Table 2 as functions of K_{loc}. The corresponding expressions for the coefficient of the leading term of the truncation error as a function of the global K and local $K_{loc} = a\Delta t_{loc}/\Delta x$ Courant numbers for $L = 1$, 3, 5 are provided in Table 3. Fig. 2 shows plots of the flux coefficients as function of K for the same values of L.

From Table 3 we conclude that for any K_{loc} the truncation error of the scheme is a

L			Flux coefficients
1	β_L	=	$-\frac{-4\,{K_{loc}}^2+{K_{loc}}^4-4\,K_{loc}-1}{8K_{loc}}$
	β_R	=	$\frac{{K_{loc}}^4-4\,{K_{loc}}^2-1+4\,Kloc}{8K_{loc}}$
3	β_L	=	$-\frac{5\,{K_{loc}}^8-5-22\,{K_{loc}}^6-50\,{K_{loc}}^2-32\,K_{loc}+40\,{K_{loc}}^4}{64K_{loc}}$
	β_R	=	$\frac{40\,{K_{loc}}^4+5\,{K_{loc}}^8-50\,{K_{loc}}^2-22\,{K_{loc}}^6+32\,K_{loc}-5}{64K_{loc}}$
5	β_L	=	$-\frac{63\,{K_{loc}}^{12}-1512\,{K_{loc}}^6+1035\,{K_{loc}}^8-63+1365\,{K_{loc}}^4-392\,{K_{loc}}^{10}-512\,K_{loc}-1008\,{K_{loc}}^2}{1024K_{loc}}$
	β_R	=	$\frac{512\,K_{loc}+63\,{K_{loc}}^{12}+1035\,{K_{loc}}^8-392\,{K_{loc}}^{10}+1365\,{K_{loc}}^4-63-1008\,{K_{loc}}^2-1512\,{K_{loc}}^6}{1024K_{loc}}$

Table 2: Flux coefficients β_L, β_R for the improved MUSTA in the case $M > L$

L	$\delta/(a\Delta x)$
1	$-\frac{K_{loc}^4-1-4\,K_{loc}^2}{8K_{loc}}-\frac{1}{2}K$
3	$-\frac{-50\,K_{loc}^2+5\,K_{loc}^8-22\,K_{loc}^6-5+40K_{loc}^4}{64K_{loc}}-\frac{1}{2}K$
5	$-\frac{-63+1365K_{loc}^4+1035K_{loc}^8-1008K_{loc}^2+63K_{loc}^{12}-392K_{loc}^{10}-1512K_{loc}^6}{1024K_{loc}}-\frac{1}{2}K$

Table 3: Normalized coefficients of the leading term of the truncation error of the improved MUSTA schemes for different L and $M > L$.

linear function of the global Courant number K and has the following form:

$$\delta = \frac{1}{2} a\Delta x \left(\psi(K_{loc}) - K\right). \tag{11}$$

From (11) we can infer the following properties of δ. Firstly, in the particular case $K_{loc} = 1$ the truncation error of the improved MUSTA is identical to that of the Godunov method. Secondly, we conclude that the truncation error of the scheme vanishes as $a \to 0$. This is a very drastic improvement over centred schemes as well as the original MUSTA scheme, for which we have $\delta \sim$ const as $a \to 0$, leading to extremely poor resolution of slowly moving waves. The improved MUSTA scheme behaves similarly to the upwind Godunov scheme for slowly moving waves, which is a desirable property of a numerical method.

We now need to choose the value of the local CFL number K_{loc} on the grounds of monotonicity. From Fig. 2 we see that the left coefficient β_L is always positive whereas the right coefficient β_R is positive in a certain interval $\xi < K_{loc} < 1$ and is negative outside it so that $\beta_R(\xi) = \beta_R(1) = 0$. Here the value of ξ depends on L and is given in Table 4. As $K_{loc} \to 1$ we see that β_R approaches zero from above. Therefore, the MUSTA scheme is not strictly monotone for the choice of the local Courant number in the interval $[\xi, 1]$. However, as the number of stages L grows, the curve of β_R becomes closer to zero for $K_{loc} \to 1$. In other words, the absolute values of β_R near $K_{loc} = 1$ diminish, see Fig.

L	1	2	3	5	10
ξ	$\sqrt{2}-1$	0.301	0.247	0.192	0.137

Table 4: Values of the smaller root ξ of the equation $\beta_R(K_{loc}) = 0$ for the improved MUSTA fluxes as a function of number of stages L, $M > L$.

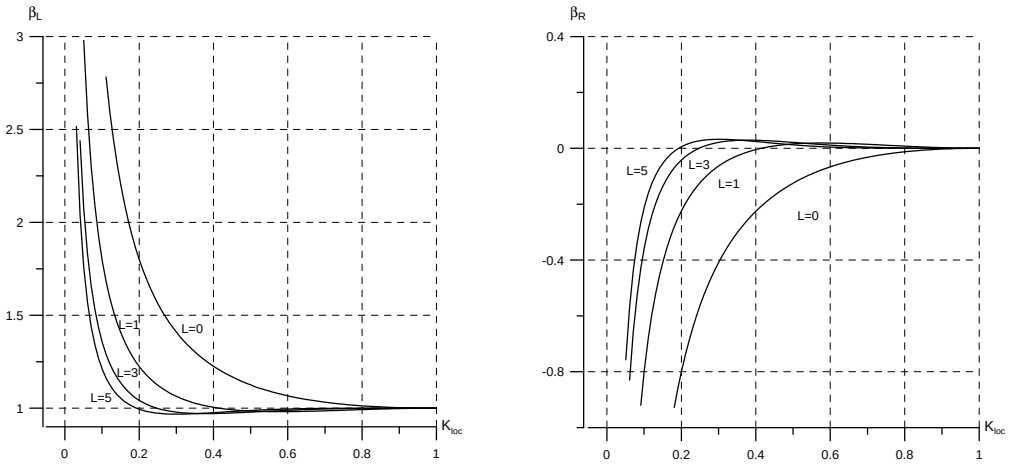

Figure 2: Plots of the flux coefficients β_L, β_R for the improved MUSTA scheme (9).

3. Since in the improved MUSTA the choice of K_{loc} can be made independently from the choice of K, it is then desirable to take K_{loc} as close to unity as possible in order to minimize the values of β_R. To be on the safe side in practical calculations, we choose $K_{loc} = 9/10$ and use this value throughout for the rest of the paper.

The truncation error of the scheme depends on K_{loc} via the function $\psi(K_{loc})$ in (11). The behavior of $\psi(K_{loc})$ for different values of L is illustrated in Fig. 4. To reproduce the Godunov method we require that ψ be equal to 1. For a given number of stages L the equation $\psi(K_{loc}) = 1$ has two real roots within the interval $[0, 1]$: $K_{loc} = \xi$ and $K_{loc} = 1$ where values of ξ are given in Table 4. We note that ξ approaches zero as L grows. For $\xi \le K_{loc} \le 1$ the truncation error of the improved MUSTA is smaller than that of the Godunov upwind scheme and therefore the MUSTA scheme loses strict monotonicity. Recall, that in this case $\beta_R > 0$. On the other hand, for $0 \le K_{loc} < \xi$ the truncation error of the improved MUSTA is larger than that of the Godunov upwind scheme and therefore the MUSTA scheme is monotone but more diffusive.

We remark that the particular choice $K_{loc} = \xi$ makes the scheme strictly monotone and identical to the Godunov scheme for the linear scalar case but for systems, either linear or nonlinear, leads to a significant decrease in accuracy. This is explained by the fact that for systems the time step is estimated using the fastest wave in the Riemann problem solution. For the slower waves the chosen time step would correspond to a smaller

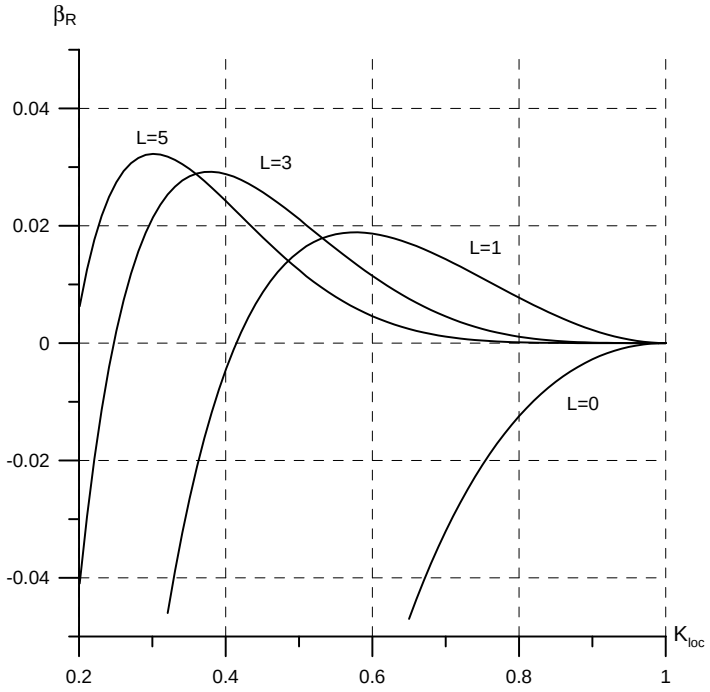

Figure 3: Plots of the right flux coefficient β_R for the improved MUSTA scheme (9) near $K_{loc} = 1$.

local Courant number, for which $\psi(K_{loc}) \to \infty$ as $K_{loc} \to 0$, as expected from the first-order centred scheme used in the local time marching (9). It is therefore desirable to choose K_{loc} as close as possible to the larger root $K_{loc} = 1$. For example, for a chosen $K_{loc} = 9/10$ the loss of strict (theoretical) monotonicity is negligible, vanishes as L grows and the truncation error tends to that of the Godunov scheme.

Table 5 contains the expressions for the coefficients of the improved MUSTA fluxes for $K_{loc} = 9/10$. We observe that as $L \to \infty$, the MUSTA flux converges to the flux of the upwind Godunov method (for $a > 0$), that is $\beta_L \to 1$ and $\beta_R \to 0$. For any given L the left flux coefficient β_L is always positive, whereas β_R is not negative but very small as compared to the original formulation, see Fig. 1. The coefficient of the leading term of the truncation error of the improved MUSTA scheme depends very weakly on the number of stages and in the limit $L \to \infty$ is equal to that of the Godunov scheme, namely $\frac{1}{2}a(1 - K)\Delta x$.

We now study the influence of the choice of the parameter M on the properties of the schemes as applied to the linear advection equation (10). Tables 6-8 list the expressions for β_L, β_R and δ for the improved MUSTA for 2, 4 and 6 cells respectively. Comparing with Table 5 we see that the presence of numerical boundaries leads to the loss of convergence to the Godunov flux starting from some stage number $l > M$. Nevertheless, the resulting flux coefficients are very close to that of the Godunov method. Moreover, the coefficient of

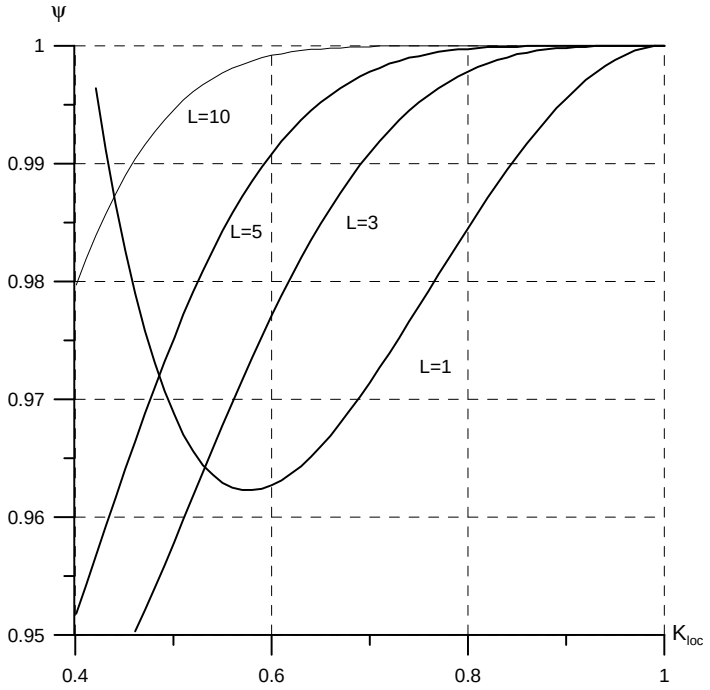

Figure 4: Plots of the function $\psi(K_{loc})$ in (11) for different number of stages L.

the leading term of the truncation error of the scheme virtually does not change (compare with Table 5) and remains a linear function of K.

5 Stability of MUSTA schemes in multiple space dimensions

In this section we study linear stability of original and improved MUSTA schemes as applied to the model linear advection equation with constant coefficients in two and three space dimensions by means of the von Neumann analysis. In the 1D case both the original and improved first-order MUSTA schemes are stable for $0 < K \leq 1$ for any number of stages $L \geq 0$. The technical details of the analysis are omitted.

For convenience we introduce the following notation: the original MUSTA scheme with L stages and two cells is denoted as MUSTA-L. The improved MUSTA scheme with $2M$ cells in the local domain size in (9) and L stages is denoted as MUSTA$_{2M}$-L. For example, MUSTA-3 corresponds to the scheme with local time marching (6) and $L = 3$ whereas MUSTA$_2$-3 corresponds to the improved MUSTA scheme with local time marching (9), $K = 9/10$ and $L = 3$.

L	β_L	β_R	$\delta/(a\Delta x)$
0	1.0027778	$-0.2777778 \times 10^{-2}$	$0.5027778 - \frac{1}{2}K$
1	0.9977639	0.2236111×10^{-2}	$0.4977639 - \frac{1}{2}K$
2	0.9995564	0.4436458×10^{-3}	$0.4995564 - \frac{1}{2}K$
3	0.9999194	0.8055556×10^{-4}	$0.4999194 - \frac{1}{2}K$
4	0.9999856	0.1441503×10^{-4}	$0.4999856 - \frac{1}{2}K$
5	0.9999974	0.2585318×10^{-5}	$0.4999974 - \frac{1}{2}K$
10	1.0000000	0.5079163×10^{-9}	$0.4999999 - \frac{1}{2}K$
15	1.0000000	$-0.2069606 \times 10^{-12}$	$0.5000000 - \frac{1}{2}K$
20	1.0000000	$0.2343364 \times 10^{-16}$	$0.5000000 - \frac{1}{2}K$

Table 5: Flux coefficients and the normalized coefficient of the leading term of the truncation error for improved MUSTA in the case $K_{loc} = 9/10$ and $M > L$.

5.1 Stability analysis in two space dimensions

Consider the following two-dimensional linear advection equation with constant coefficients

$$\frac{\partial}{\partial t}q + \frac{\partial}{\partial x}f(q) + \frac{\partial}{\partial y}g(q) = 0, \quad f = aq, \quad g = bq.$$

Here the coefficients a, b are constant and positive. The scheme (3) now reads

$$q_{ij}^{n+1} = q_{ij}^{n} - \frac{\Delta t}{\Delta x}\left(f_{i+1/2,j} - f_{i-1/2,j}\right) - \frac{\Delta t}{\Delta y}\left(g_{ij+1/2} - g_{ij-1/2}\right). \tag{12}$$

To perform the von Neumann stability analysis of our schemes we first rewrite (12) in the following form:

$$q_{ij}^{n+1} = \sum_{l,m=-1}^{1} b_{lm} q_{i+l,j+m}^{n}, \tag{13}$$

where b_{lm} are the coefficients of the schemes. We then consider a *trial solution* $q_{ij}^{n} = S^n \exp\left(I(i\alpha + j\beta)\right.$, where α and β are phase angles in x and y directions. Inserting the trial solution into (12) we obtain the following algebraic expression for the modulus of the amplification factor S:

$$|S|^2 = \left(\sum_{l,m=-1}^{1} b_{lm}\cos\left(l\alpha + m\beta\right)\right)^2 + \left(\sum_{l,m=-1}^{1} b_{lm}\sin\left(l\alpha + m\beta\right)\right)^2. \tag{14}$$

For linear stability we impose the condition $|S| \leq 1$. Since the resulting expression for $|S|$ is intractable for algebraic analysis we adopt the idea of verifying the condition $|S| \leq 1$ numerically rather than analytically [17] as follows. Let us define Courant numbers for

L	β_L	β_R	$\delta/(a\Delta x)$
1	0.9977639	0.2236111×10^{-2}	$0.4977639 - \frac{1}{2}K$
2	0.9972876	0.2712431×10^{-2}	$0.4972876 - \frac{1}{2}K$
3	0.9972423	0.2757681×10^{-2}	$0.4972423 - \frac{1}{2}K$
4	0.9972380	0.2761979×10^{-2}	$0.4972380 - \frac{1}{2}K$
5	0.9972376	0.2762388×10^{-2}	$0.4972376 - \frac{1}{2}K$
10	0.9972376	0.2762431×10^{-2}	$0.4972376 - \frac{1}{2}K$
15	0.9972376	0.2762431×10^{-2}	$0.4972376 - \frac{1}{2}K$

Table 6: Flux coefficients and the normalized coefficient of the leading term of the truncation error for improved MUSTA in the case $K_{loc} = 9/10$ and $M = 1$ (2 cells).

L	β_L	β_R	$\delta/(a\Delta x)$
2	0.9995564	$+0.4436458 \times 10^{-3}$	$0.4995564 - \frac{1}{2}K$
3	0.9999195	$+0.8045226 \times 10^{-4}$	$0.4999195 - \frac{1}{2}K$
4	0.9999805	$+0.1953398 \times 10^{-4}$	$0.4999805 - \frac{1}{2}K$
5	0.9999904	$+0.9598415 \times 10^{-5}$	$0.4999904 - \frac{1}{2}K$
10	0.9999923	$+0.7673518 \times 10^{-5}$	$0.4999923 - \frac{1}{2}K$
15	0.9999923	$+0.7673302 \times 10^{-5}$	$0.4999923 - \frac{1}{2}K$

Table 7: Flux coefficients and the normalized coefficient of the leading term of the truncation error for improved MUSTA in the case $K_{loc} = 9/10$ and $M = 2$ (4 cells).

each coordinate direction as $K_x = a\Delta t/\Delta x$, $K_y = b\Delta t/\Delta y$. For a given pair (K_x, K_y), we evaluate the amplification factor $S(K_x, K_y, \alpha, \beta)$ for many phase angles α, β and record the proportion $p(K_x, K_y)$ of these pair for which $|S| \leq 1$. Then a contour plot of $p(K_x, K_y)$ in the $K_x - K_y$ plane will indicate the stability region of the scheme.

Fig. 5 shows the stability plots of the original MUSTA scheme [15, 16] for one and three stages. We observe that the stability region depends on the number of stages and in general diminishes when L grows. For $L = 1$ it can be approximately described by the following inequality:

$$(K_x)^2 + (K_y)^2 \leq \left(\frac{3}{4}\right)^2.$$

We note that the truncation error of the original MUSTA is inversely proportional to Courant numbers in x and y coordinate directions and thus does not vanish when either of coefficients a, b is equal to zero. As a result, the schemes do not recover the one-

L	β_L	β_R	$\delta/(a\Delta x)$
2	0.9995564	$+0.4436458 \times 10^{-3}$	$0.4995564 - \frac{1}{2}K$
3	0.9999195	$+0.8045226 \times 10^{-4}$	$0.4999195 - \frac{1}{2}K$
4	0.9999856	$+0.1441503 \times 10^{-4}$	$0.4999856 - \frac{1}{2}K$
5	0.9999974	$+0.2585318 \times 10^{-5}$	$0.4999974 - \frac{1}{2}K$
6	0.9999995	$+0.4769698 \times 10^{-6}$	$0.4999995 - \frac{1}{2}K$
7	0.9999999	$+0.1021531 \times 10^{-6}$	$0.4999999 - \frac{1}{2}K$
10	1.0000000	$+0.2170712 \times 10^{-7}$	$0.5000000 - \frac{1}{2}K$
15	1.0000000	$+0.2125592 \times 10^{-7}$	$0.5000000 - \frac{1}{2}K$

Table 8: Flux coefficients and the normalized coefficient of the leading term of the truncation error for improved MUSTA in the case $K_{loc} = 9/10$ and $M = 3$ (6 cells).

dimensional stability condition $0 \leq K \leq 1$ when one of the advection coefficients is zero. This is especially evident for $L = 1$.

Fig. 6 shows the stability contour plots of $p(K_x, K_y)$ for the first-order Godunov and MUSTA$_2$-1 schemes of the form (12). These plots look very similar and the stability regions can be approximately written as

$$K_x + K_y \leq 1,$$

which is larger than that of the original MUSTA schemes. The stability plots of the improved MUSTA schemes with a large number of stages L or cells $2M$ are virtually identical to those in the Fig. 6 and are thus omitted.

5.2 Stability analysis in three space dimensions

Consider the three-dimensional linear equation with constant coefficients

$$\frac{\partial}{\partial t}q + \frac{\partial}{\partial x}f(q) + \frac{\partial}{\partial y}g(q) + \frac{\partial}{\partial z}h(q) = 0, \quad f = aq, \quad g = bq, \quad h = cq.$$

Here the coefficients a, b, c are constant and positive. The scheme now reads

$$\begin{aligned} q_{ijk}^{n+1} = q_{ijk}^{n} - \frac{\Delta t}{\Delta x}\left(f_{i+1/2,jk} - f_{i-1/2,jk}\right) \\ -\frac{\Delta t}{\Delta y}\left(g_{ij+1/2,k} - g_{ij-1/2,k}\right) - \frac{\Delta t}{\Delta z}\left(h_{ijk+1/2} - h_{ijk-1/2}\right), \end{aligned} \tag{15}$$

or in a more concise form:

$$q_{ijk}^{n+1} = \sum_{l,m,p=-1}^{1} b_{lmp} q_{i+l,j+m,k+p}^{n}.$$

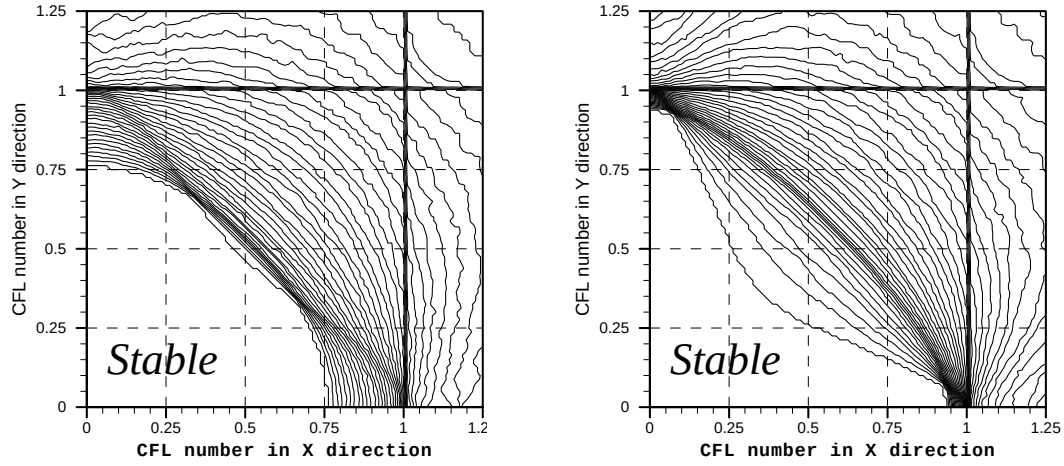

Figure 5: Stability regions for two-dimensional unsplit MUSTA schemes from [15, 16]. Left: MUSTA-1, right: MUSTA-3.

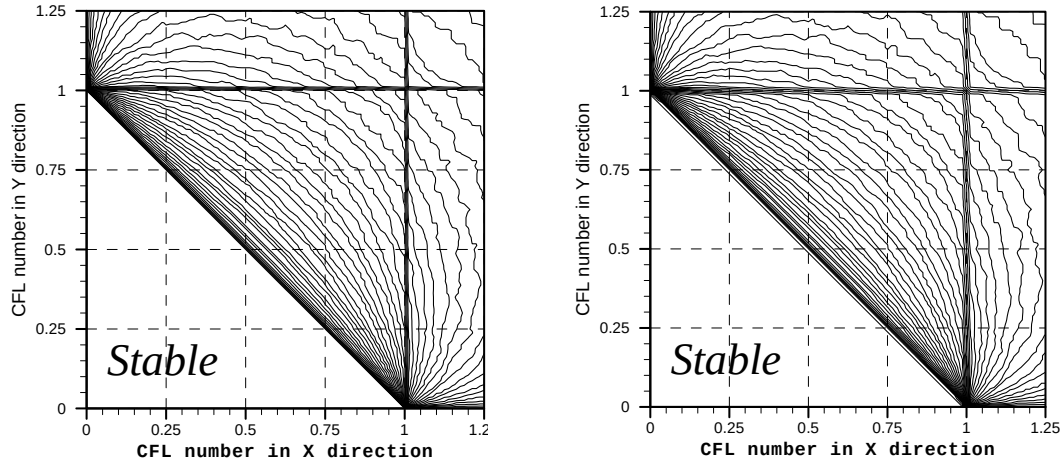

Figure 6: Stability regions for two-dimensional unsplit schemes. Left: Godunov scheme, right: MUSTA$_2$-1 scheme.

The expression for the modulus of the amplification factor S is then given by:

$$|S|^2 = \left(\sum_{l,m,p=-1}^{1} b_{lmp} \cos\left(l\alpha + m\beta + p\gamma\right) \right)^2 + \left(\sum_{l,m,p=-1}^{1} b_{lmp} \sin\left(l\alpha + m\beta + p\gamma\right) \right)^2 ,$$

where α, β, γ are the phase angles. For linear stability we impose the condition $|S| \leq 1$ and study it by plotting counters of $p(K_x, K_y, , K_Z)$ in $K_x - K_y$ plane for different values of $K_z = c\Delta t/\Delta z$.

Fig. 7 shows stability plots for the Godunov method for $K_z = 0$ and $1/3$. The corresponding plots for the MUSTA$_2$-1 scheme are given in Fig. 8. The stability regions of both schemes are very similar and can be approximately written as

$$K_x + K_y + K_z \leq 1.$$

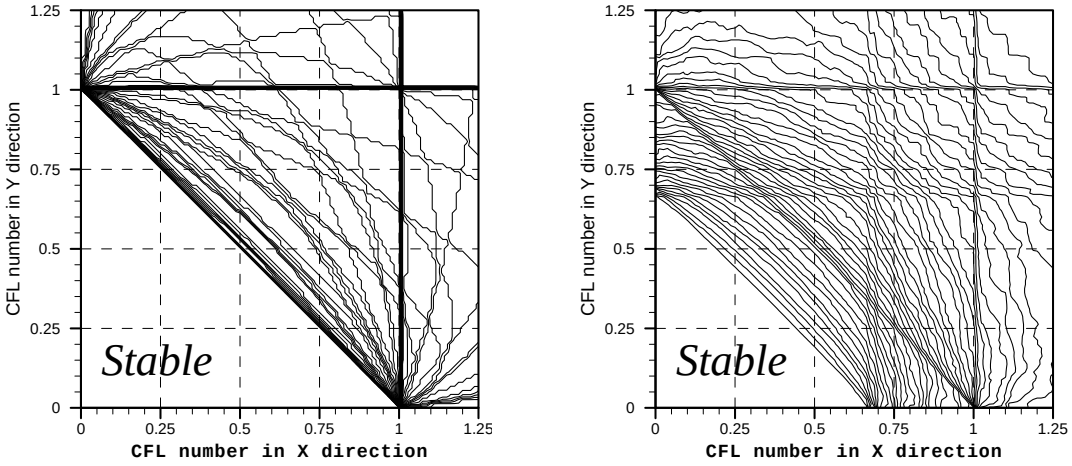

Figure 7: Stability regions for the three-dimensional Godunov scheme for $K_z = 0$ (left plot) and $K_z = 1/3$ (right plot).

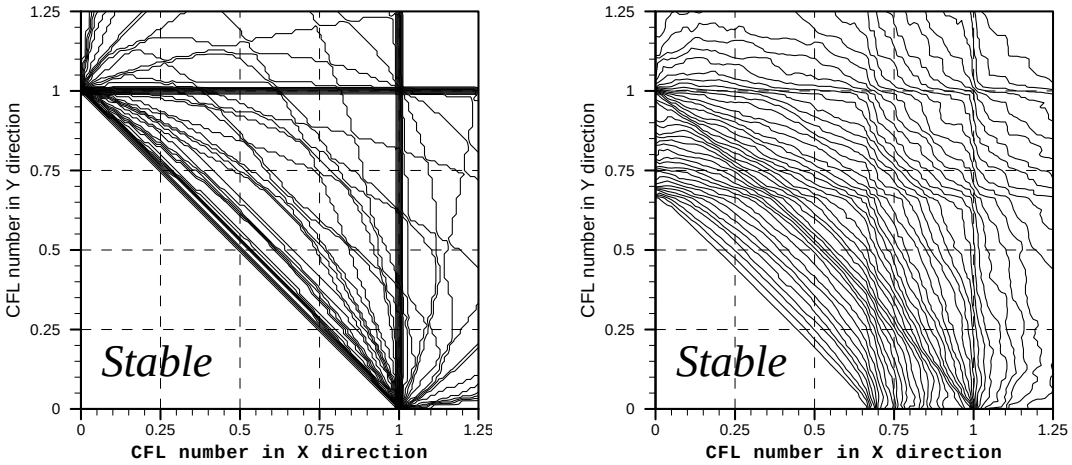

Figure 8: Stability regions for the three-dimensional MUSTA$_2$-1 scheme for $K_z = 0$ (left) and $K_z = 1/3$ (right).

The stability plots of the original MUSTA-1 scheme in three space dimensions are given in Fig. 9. We observe that the stability region is again smaller than that of improved MUSTA schemes of the present paper and the Godunov scheme and can be approximately written as is

$$(K_x)^2 + (K_y)^2 + (K_z)^2 \leq \frac{3}{5}.$$

Therefore, we have established that of the unsplit versions of MUSTA schemes are stable in multiple space dimensions. In particular, the stability region of improved MUSTA schemes coincides with that of the unsplit Godunov method. This allows us to use the MUSTA flux as a building block in many existing high-order schemes, such as MUSCL-type TVD schemes [5, 20, 2] and essentially non-oscillatory scheme [11]. We remind the

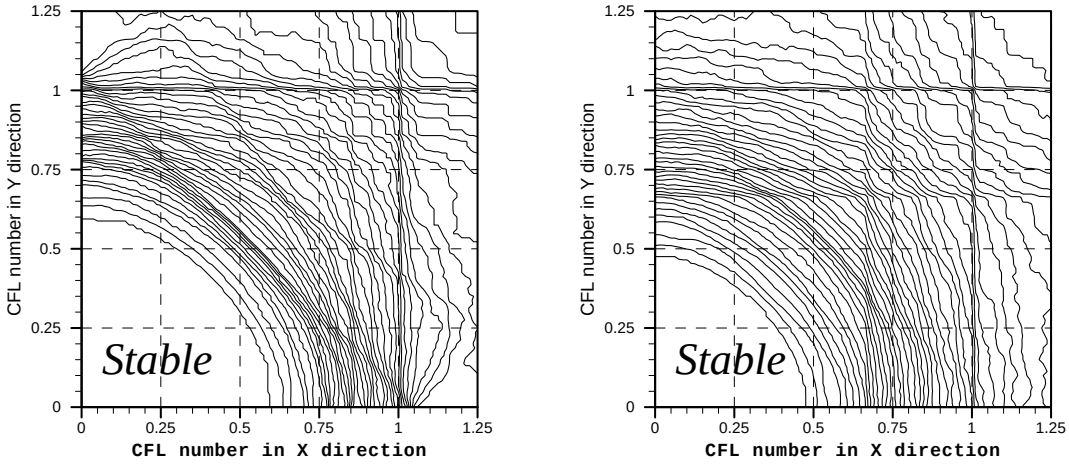

Figure 9: Stability regions for the three-dimensional MUSTA-1 scheme from [15, 16] for $K_z = 0$ (left) and $K_z = 1/3$ (right).

reader that the use of centred fluxes is the unsplit Godunov schemes of the form (3) leads to unconditionally unstable finite-volume methods [17].

6 Practical implementation for nonlinear systems

Practical application of the MUSTA approach to nonlinear systems requires a particular choice of the number of stages L in the local time marching. Since discussion for the original MUSTA is found in [15, 16] here we concentrate on the improved MUSTA schemes for which we additionally have to specify the number of cells $2M$ in the local spatial domain. As was shown above, the choice of L determines how close the resulting MUSTA flux is to the Godunov flux. The choice of the parameter M in the improved MUSTA schemes also affects the convergence of the flux to the optimal upwind Godunov flux.

We first discuss the dependence of monotonicity of the MUSTA flux on the number of stages L. Recall that the definition of monotone schemes applies only to scalar equations. When applied to nonlinear systems, these schemes, though monotone in the one-dimensional scalar case, may produce oscillations due to the non-linearity of the system to be solved. Probably, the most well-known example is the generation of oscillations by first-order Godunov methods behind slowly moving shock waves. Therefore, from the practical point of view a slight loss of monotonicity of the flux for a small number of stages L, evident in Table 5, is not important. In practical computations the one-stage scheme ($L = 1$), for which $\beta_R \approx 2 \times 10^{-3}$ produces perfectly non-oscillatory results even for very severe test problems, such as blast wave interaction and double Mach reflection problems from [21], see section of numerical results below.

For large values of L, however, reflections from the numerical boundaries may affect the local time marching and the structure of the self-similar solution leading to less robust schemes. It may still be possible to use L larger than M, but not much larger. The actual value of L allowed for a given M does depend on the problem at hand. For example, our experiments for the Euler equations show that for 2 cells it is safe to use $L \leq 3$. For a large number of stages the use of four and more cells is recommended on the grounds of monotonicity and robustness.

For the linear advection equation the choice of L and M defines monotonicity properties of the flux but virtually does not affect the accuracy. For non-linear systems, however, the accuracy of the improved MUSTA schemes does depend on the choice of L. In general, for complicated systems with many waves it may be necessary to take L relatively large in order to resolve the structure of the self-similar solution of the local Riemann problem (4) and to pick up the correct flux value at the interface position. The choice of L, which gives the best accuracy, then depends on the system to be solved and should be determined empirically. For the compressible Euler equations, see section of numerical results, the choice $L = 3$ seems to produce good results in most cases.

A remark is in order on the practical implementation of the flux for large values of L and M. Note that the waves emerging from the interface position $x_{i+1/2}$ in the local Riemann problem have travelled only l cells in both directions at stage l. Therefore, a considerable reduction of computational cost can be achieved if one carries out the actual update in (9) for a given stage l only for cells $-l+1 \leq m \leq l$ rather than over the entire local domain $-M+1 \leq m \leq M$.

7 Numerical results

In this section we present numerical results illustrating the performance of the improved MUSTA schemes of the present paper in one, two and three space dimensions as applied to the compressible Euler equations for a gamma-law gas, which have the form (1) with:

$$\mathbf{Q} = \begin{pmatrix} \rho \\ \rho u \\ \rho v \\ \rho w \\ E \end{pmatrix}, \quad \mathbf{F} = \mathbf{Q}u + \begin{pmatrix} 0 \\ p \\ 0 \\ 0 \\ pu \end{pmatrix}, \quad \mathbf{G} = \mathbf{Q}v + \begin{pmatrix} 0 \\ 0 \\ p \\ 0 \\ pv \end{pmatrix}, \quad \mathbf{H} = \mathbf{Q}w + \begin{pmatrix} 0 \\ 0 \\ 0 \\ p \\ pw \end{pmatrix} \tag{16}$$

$$p = (\gamma - 1)(E - \frac{1}{2}\rho(u^2 + v^2 + w^2)),$$

where ρ, u, v, w p and E are density, components of velocity in the x, y and z coordinate directions, pressure and total energy, respectively; γ is the ratio of specific heats, we use $\gamma = 1.4$ throughout.

The section is divided into two parts. In the first part we study the performance of MUSTA by using it as a building block in the basic first-order finite-volume scheme (3) in one and three space dimensions. We compare results of MUSTA with those of the Godunov scheme with the exact Riemann solver. As was already mentioned, the scheme with the exact Riemann solver is the most accurate one and therefore should be used as a reference scheme for comparisons. Additionally, we compare MUSTA with a state-of-art HLL Riemann solver [4] in order to demonstrate how it fairs against other modern and popular upwind schemes. In one space dimension we have also run the centred Lax-Friedrichs scheme [8], but the results were found to be significantly inferior to that of MUSTA and HLL schemes and are thus omitted.

In the second part we use MUSTA as a building block in the state-of-art weighted essentially non-oscillatory (WENO) schemes of semi-discrete form (2) for a couple of two-dimensional test problems: a vortex evolution problem [11] and a double Mach reflection problem [21]. In calculations we run a particular two-dimensional variant of the WENO scheme from [12], which uses a two-point Gaussian quadrature instead of a three point one as done in [11].

For the compressible Euler equations (16) we find that the most economical variant of MUSTA with 2 cells ($M = 2$) and a small number of stages $L \leq 3$ produces good results. We therefore limit our presentation of MUSTA to the particular variants: original MUSTA-3 and improved MUSTA_2-1 and MUSTA_2-3.

7.1 First-order MUSTA schemes

7.1.1 Blast wave interaction problem

We solve the blast wave interaction test problem from [21] for the one-dimensional Euler equations. The initial condition defined on $[0 : 1]$ consists of three regions of gas at rest between reflecting walls. Density is unity everywhere, whereas pressure is given by

$$p = \begin{cases} 1000, & 0.0 \leq x \leq 0.1, \\ 0.01, & 0.1 \leq x \leq 0.9, \\ 100, & 0.9 \leq x \leq 1.0. \end{cases}$$

A detailed study of the flow physics can be found in [21]. As time evolves, two blast waves emerge and collide, resulting in a very complex flow pattern. This test problem is suitable to test the performance of the numerical schemes, in particular their robustness,

due to the extreme magnitudes of waves.

Here we present results of different methods on a mesh of 3000 cells and with Courant number $K = 0.9$. For all runs we also plot (with a dashed line) a very accurate reference solution obtained by running a high-order scheme on a very fine mesh. For comparisons we select two most delicate flow variables: density and internal energy $e = \frac{p}{(\gamma-1)\rho}$. Other variables such as velocity and pressure do not reveal the inaccuracy of the computations.

Figs. 10–11 show results of MUSTA$_2$-1 and MUSTA$_2$-3 schemes (circles) as compared with the Godunov method with the exact Riemann solver (solid line) at the final time $t = 0.038$. In Fig. 10 we observe that MUSTA$_2$-1 produces profiles which are already quite close to those of the exact Riemann solver. Next, in Fig. 11, the MUSTA$_2$-3 scheme matches the performance of the exact Riemann solver. Fig. 12 depicts results of MUSTA$_2$-3 (solid line) as compared with the state-of-the art HLL scheme (circles). It is obvious from the figure that the HLL solution agrees with the MUSTA solutions for shock waves but is more diffusive for the more delicate contact discontinuities, especially for the left-going one. This is more clearly seen on the internal energy plot.

Finally, we demonstrate the difference in accuracy between improved MUSTA (developed in this paper) and original MUSTA by performing a computation with a *smaller* (global) Courant number equal to $K = 0.2$. On Fig. 13 we plot results of the improved MUSTA$_2$-3 (solid line) and original MUSTA-3 (circles) schemes. It is clear that the accuracy of the MUSTA$_2$-3 scheme does not decrease significantly when a smaller Courant number is used, compare with Fig. 12. The accuracy of the original MUSTA-3 does decrease and is worse than that of the MUSTA$_2$-3 scheme. We note, however, that the original MUSTA is still much superior to a typical centred scheme for this test problem.

The observed difference in accuracy between original and improved MUSTA schemes is explained by the fact that the truncation error of the original MUSTA is inversely proportional to the Courant number whereas for the improved MUSTA of this paper it is a linear function of the Courant number. Therefore, for large Courant numbers, close to unity, the performance of original and improved MUSTA schemes is similar whereas for small Courant numbers the improved one is superior.

7.1.2 Three-dimensional explosion test problem [14]

We solve the three-dimensional Euler equations for a gamma-law gas (16). The initial condition defined on $[-1:1] \times [-1:1] \times [-1:1]$ consists of two regions of constant but different values of gas parameters separated by a sphere of radius 0.4:

$$(\rho, p) = \begin{cases} (1.0,\ 1.0), & r \le 0.4 \\ (0.125,\ 0.1), & r > 0.4 \end{cases}, \quad u = v = w = 0, \quad r^2 = x^2 + y^2 + z^2. \tag{17}$$

This initial condition corresponds to the so-called spherical explosion test problem [14]. We compute the numerical solution at the output time $t = 0.25$ on a mesh of 101 cells in each coordinate direction. We use $K = 0.3$ for all runs, where $K = \max(K_x, K_y, K_z)$. Recall, that for the linear advection equation the schemes are stable for $K_x + K_y + K_z \leq 1/3$. As in the one-dimensional study, we denote by a dashed line a reference (radial) solution, which is obtained by solving the one-dimensional Euler equations with a geometric source term on a very fine mesh. See Section 17.1 of [14] for details.

Fig. 14 shows a comparison of results of MUSTA$_2$-3 and the Godunov scheme with the exact Riemann solver. We present distributions of gas density and internal energy along the x axis. The solution contains a spherical shock wave and a contact surface travelling away from the centre and a spherical rarefaction wave travelling towards the origin (0,0,0). We observe that the accuracy of MUSTA$_2$-3 is virtually identical to that of the Godunov scheme with the exact Riemann solver. Fig. 15 shows a comparison of the MUSTA$_2$-3 and HLL schemes. As in the one-dimensional case, the HLL solver is somewhat less accurate, especially near the origin.

We have also run a special test case of a stationary contact discontinuity, for which centred schemes as well as upwind schemes with incomplete Riemann solvers (e.g. HLL scheme) are known to produce inaccurate results [14] whereas the Godunov scheme with the exact Riemann solver or a complete Riemann solver (e.g. HLLC Riemann solver [19]) resolve the stationary contact discontinuity exactly. In such situations MUSTA schemes generally converge to the exact solution as $L \to \infty$, $M > L$. Typically, for $L \geq 10$ the MUSTA results can be regarded as converged. However, the particular variants with $L = 1, \ldots, 3$ stages are less accurate than the Godunov scheme with the exact Riemann solver but much more accurate than HLL [4] or Lax-Friedrichs [8] schemes.

7.2 WENO-MUSTA schemes

We now illustrate the application of MUSTA fluxes to finite-volume weighted essentially non-oscillatory (WENO) schemes [11] in two space dimensions. We use a variant of the scheme [12] with two Gaussian integration points along the cell side. In all examples fifth-order reconstruction and third-order time integrations are used, see [11, 12] for details.

7.2.1 Vortex evolution problem

We solve the two-dimensional Euler equations with the initial conditions, corresponding to a smooth vortex, moving at 45^o to the Cartesian mesh lines in the square domain $[-5:5] \times [-5:5]$, see [11]. We apply periodic boundary conditions. The vortex is defined as the following isentropic perturbation to the uniform flow of unit values of primitive

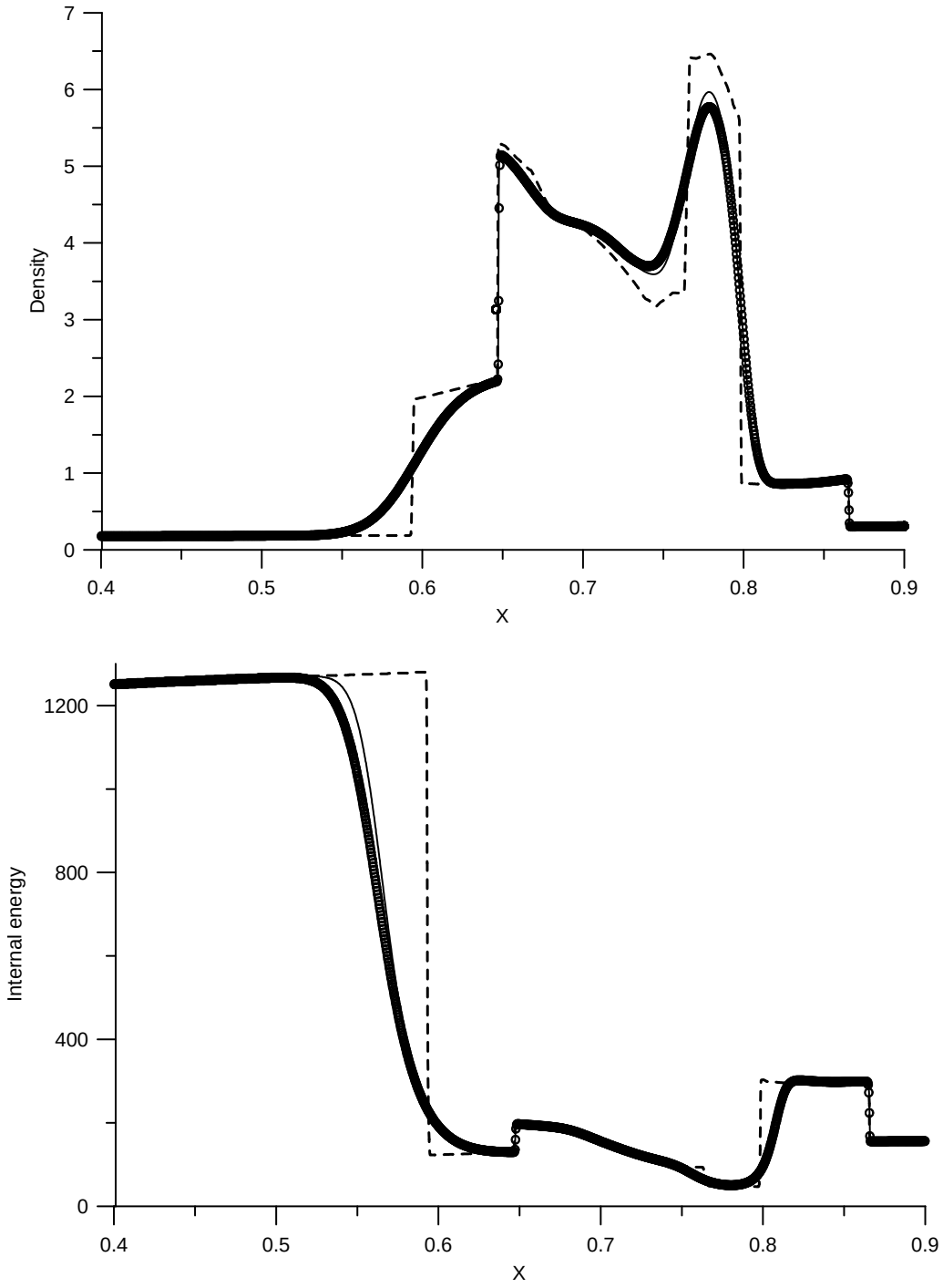

Figure 10: Blast wave interaction problem. CFL=0.9. Dashed line – reference solution, solid line – the Godunov scheme with the exact Riemann solver, circles – MUSTA$_2$-1.

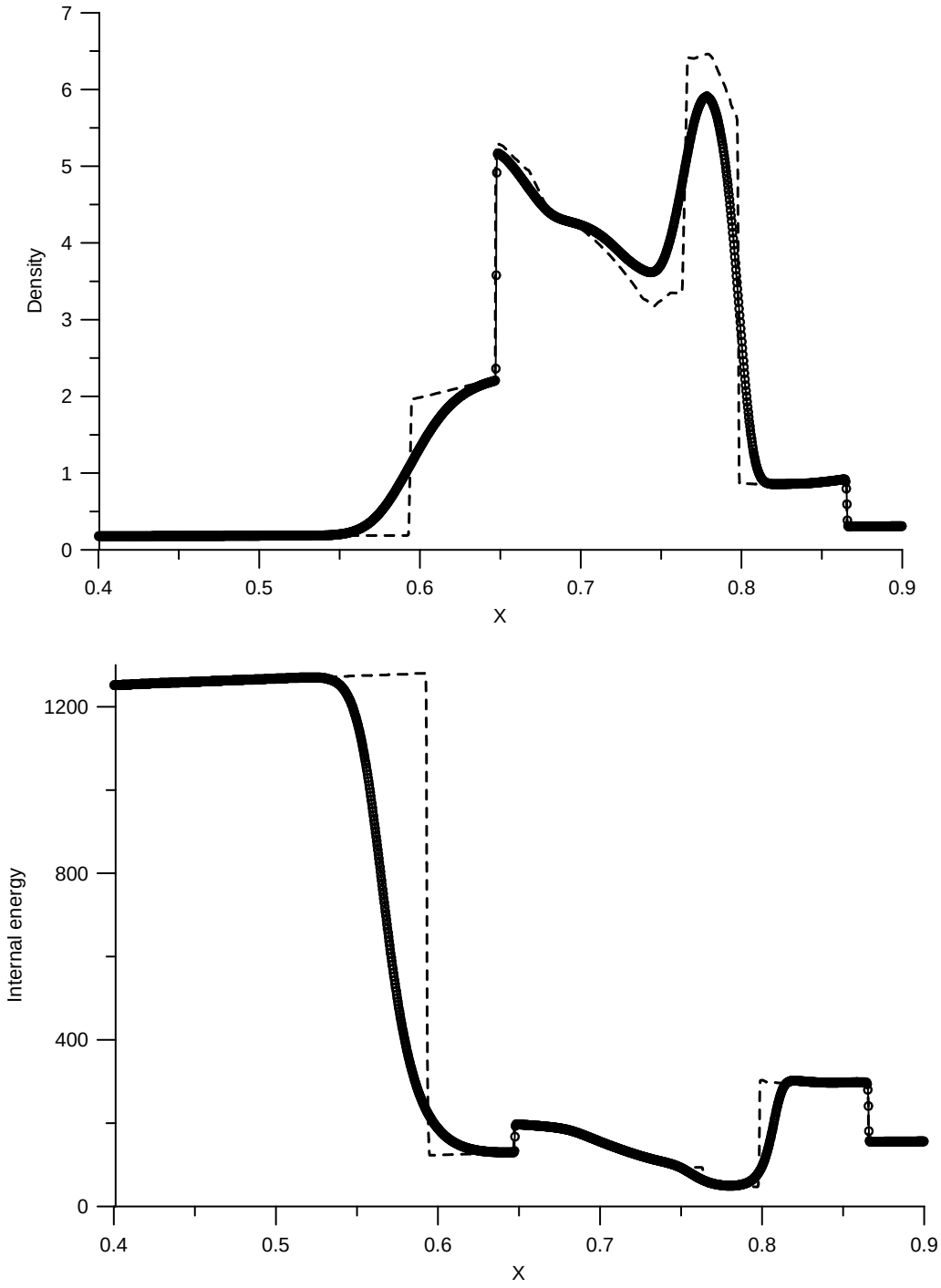

Figure 11: Blast wave interaction problem. CFL=0.9. Dashed line – reference solution, solid line – the Godunov scheme with the exact Riemann solver, circles – MUSTA$_2$-3.

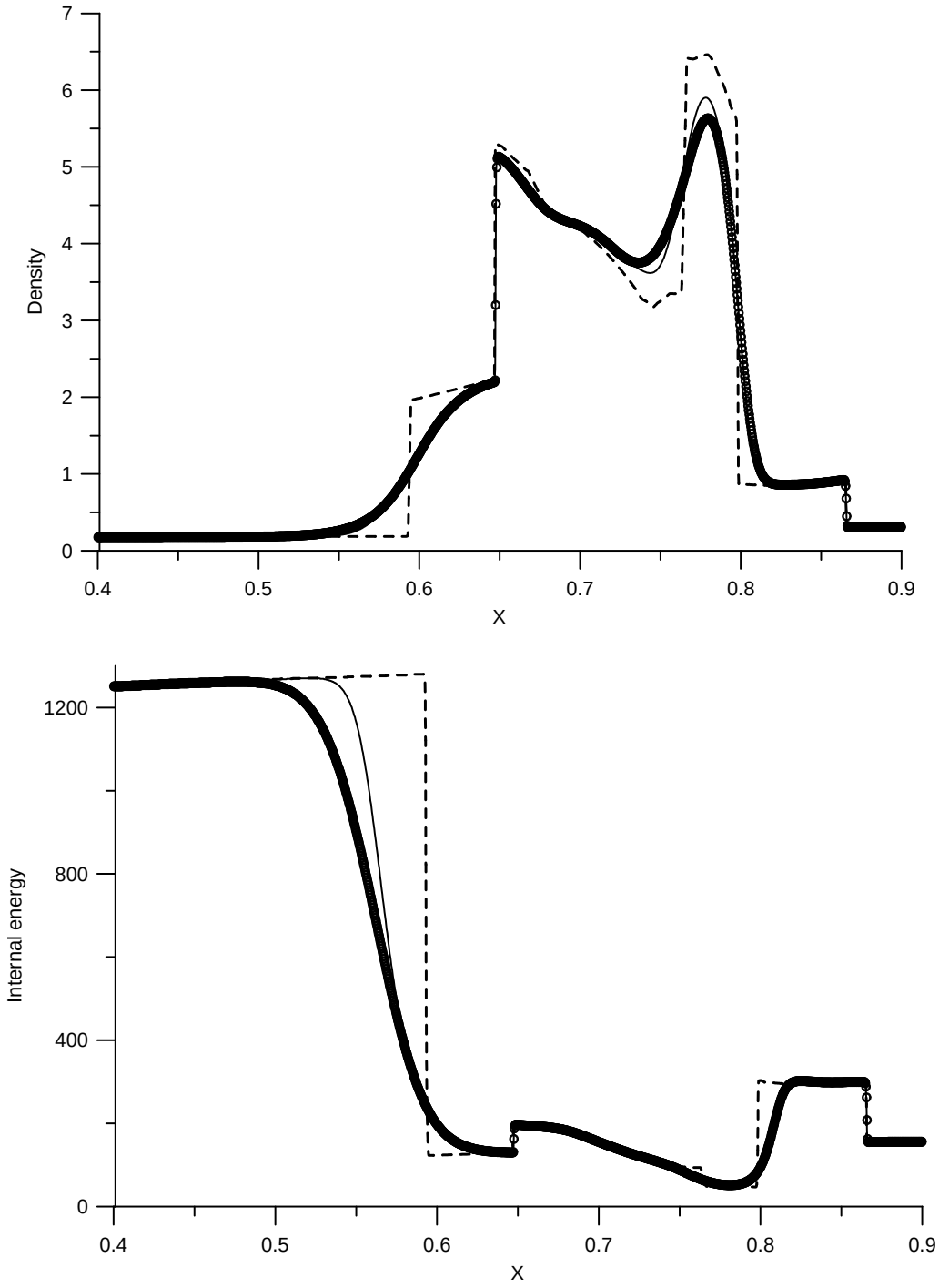

Figure 12: Blast wave interaction problem. CFL=0.9. Dashed line – reference solution, solid line – MUSTA$_2$-3, circles – the Godunov scheme with the HLL solver.

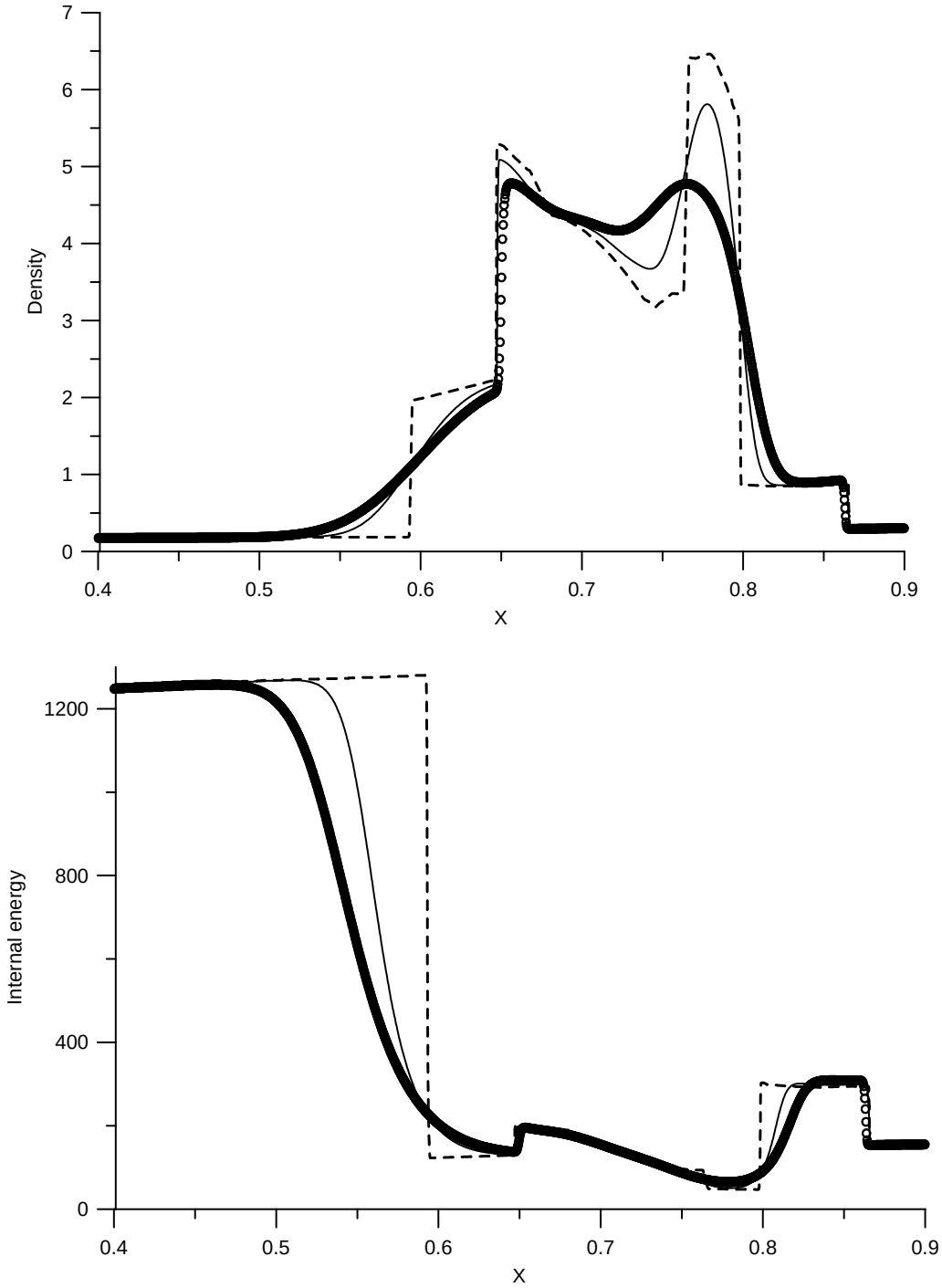

Figure 13: Blast wave interaction problem. CFL=0.2. Dashed line – reference solution, solid line – present MUSTA$_2$-3, circles – original MUSTA-3 from [15, 16].

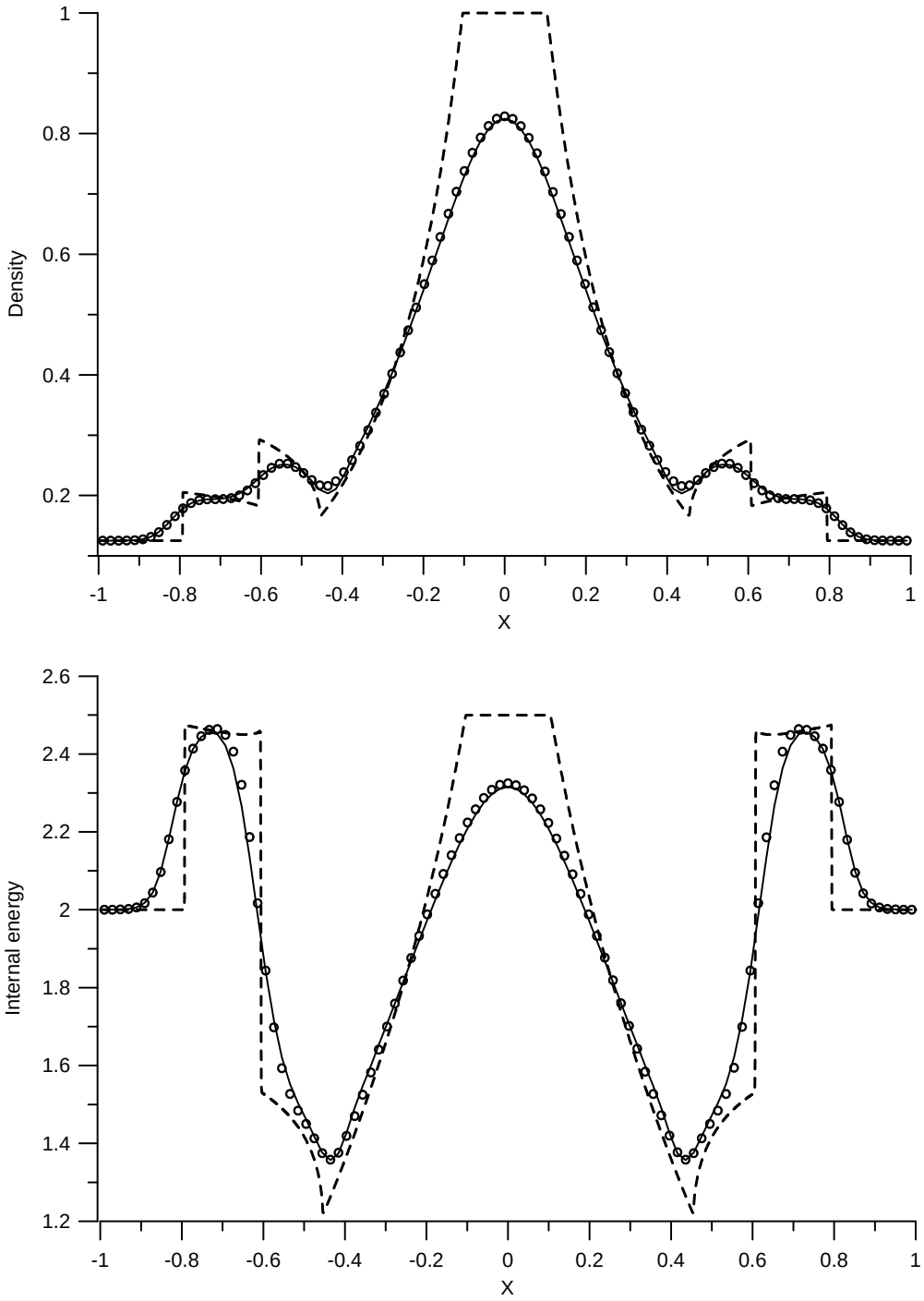

Figure 14: Three-dimensional explosion problem. Dashed line – reference solution, solid line – the Godunov scheme with the exact Riemann solver, circles – MUSTA$_2$-3.

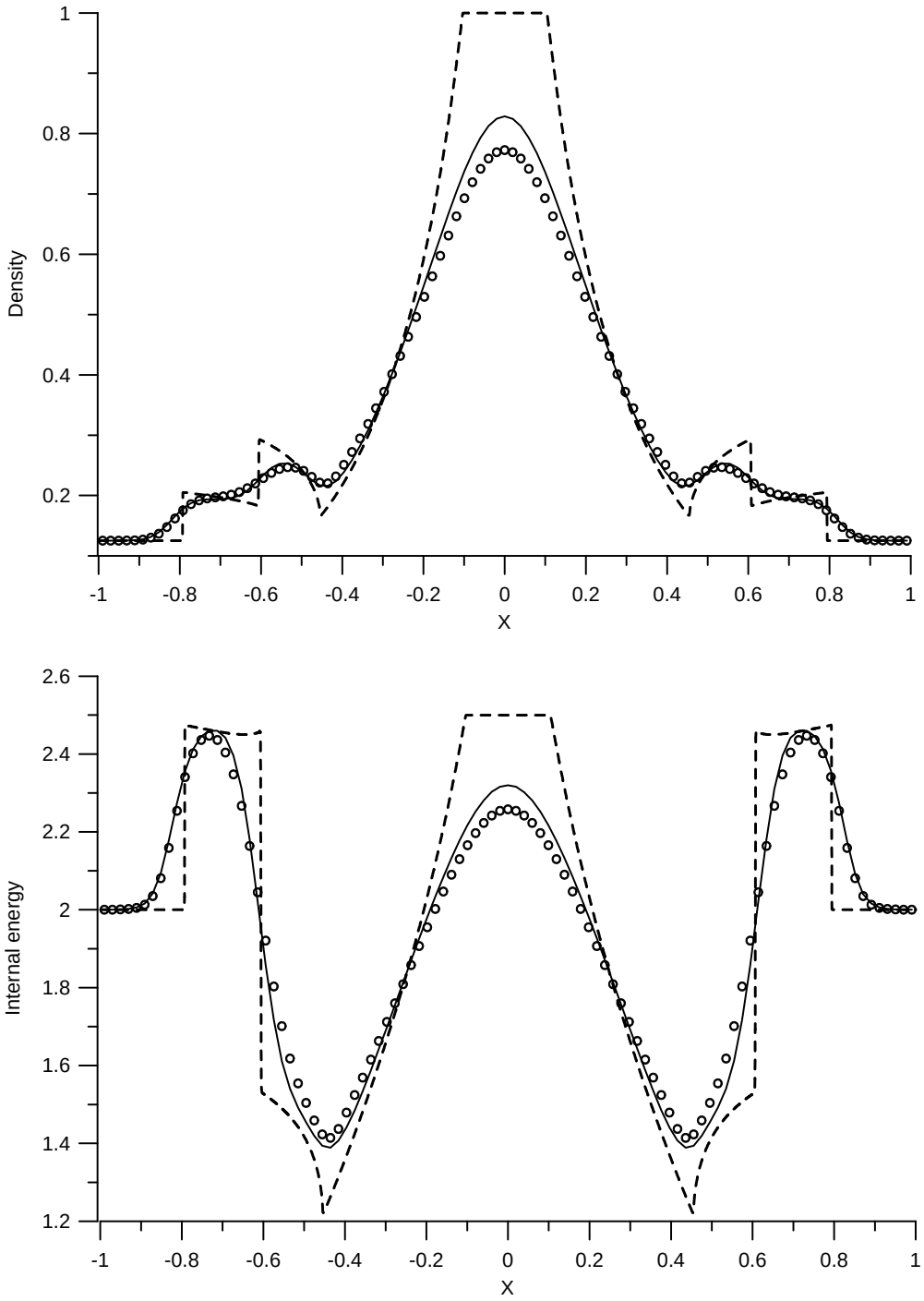

Figure 15: Three-dimensional explosion problem. Dashed line – reference solution, solid line – MUSTA$_2$-3, circles – the Godunov scheme with the HLL Riemann solver.

variables:

$$u = 1 - \frac{\varepsilon}{2\pi} e^{\frac{1}{2}(1-r^2)}\, y, \quad v = 1 + \frac{\varepsilon}{2\pi} e^{\frac{1}{2}(1-r^2)}\, x,$$
$$T = 1 - \frac{(\gamma-1)\varepsilon^2}{8\gamma\pi^2} e^{(1-r^2)}, \quad \frac{p}{\rho^\gamma} = 1, \tag{18}$$

where $r^2 = x^2 + y^2$ and the vortex strength is $\varepsilon = 5$. We compute the numerical solution at the output time $t = 10$ which corresponds to one time period; at this time the vortex returns to the initial position. We use $K = 0.45$ for all runs.

Table 9: Density convergence study for the vortex evolution problem (18)

Method	Mesh	L_∞ error	L_∞ order	L_1 error	L_1 order
Exact Riemann solver	25×25	6.61×10^{-2}		3.85×10^{-3}	
	50×50	9.89×10^{-3}	2.74	2.76×10^{-4}	3.80
	100×100	2.68×10^{-4}	5.21	1.24×10^{-5}	4.47
HLL	25×25	6.86×10^{-2}		4.32×10^{-3}	
	50×50	1.00×10^{-2}	2.78	2.93×10^{-4}	3.88
	100×100	2.84×10^{-4}	5.14	1.39×10^{-5}	4.40
MUSTA$_2$-1	25×25	7.96×10^{-2}		5.12×10^{-3}	
	50×50	1.17×10^{-2}	2.77	3.45×10^{-4}	3.89
	100×100	3.52×10^{-4}	5.06	1.66×10^{-5}	4.38
MUSTA$_2$-3	25×25	6.20×10^{-2}		3.62×10^{-3}	
	50×50	9.70×10^{-3}	2.68	2.62×10^{-4}	3.79
	100×100	2.56×10^{-4}	5.25	1.12×10^{-5}	4.54

Table 9 shows the convergence study for schemes with different fluxes. The errors of cell averages of the solution in L_∞ and L_1 norms are presented. We observe that approximately fifth order convergence rate is achieved. Schemes with MUSTA$_2$-3 and exact Riemann solver produce similar errors whereas those with HLL and MUSTA$_2$-1 are somewhat less accurate. The difference in accuracy can be explained as follows. The HLL Riemann solver does not recognize all the waves in the Riemann problem solution and is thus more diffusive than the exact (complete) Riemann solver. Although the MUSTA$_2$-1 flux does attempt to resolve all the waves by local time marching, one stage is obviously not sufficient to do so accurately, whereas the MUSTA$_2$-3 does it.

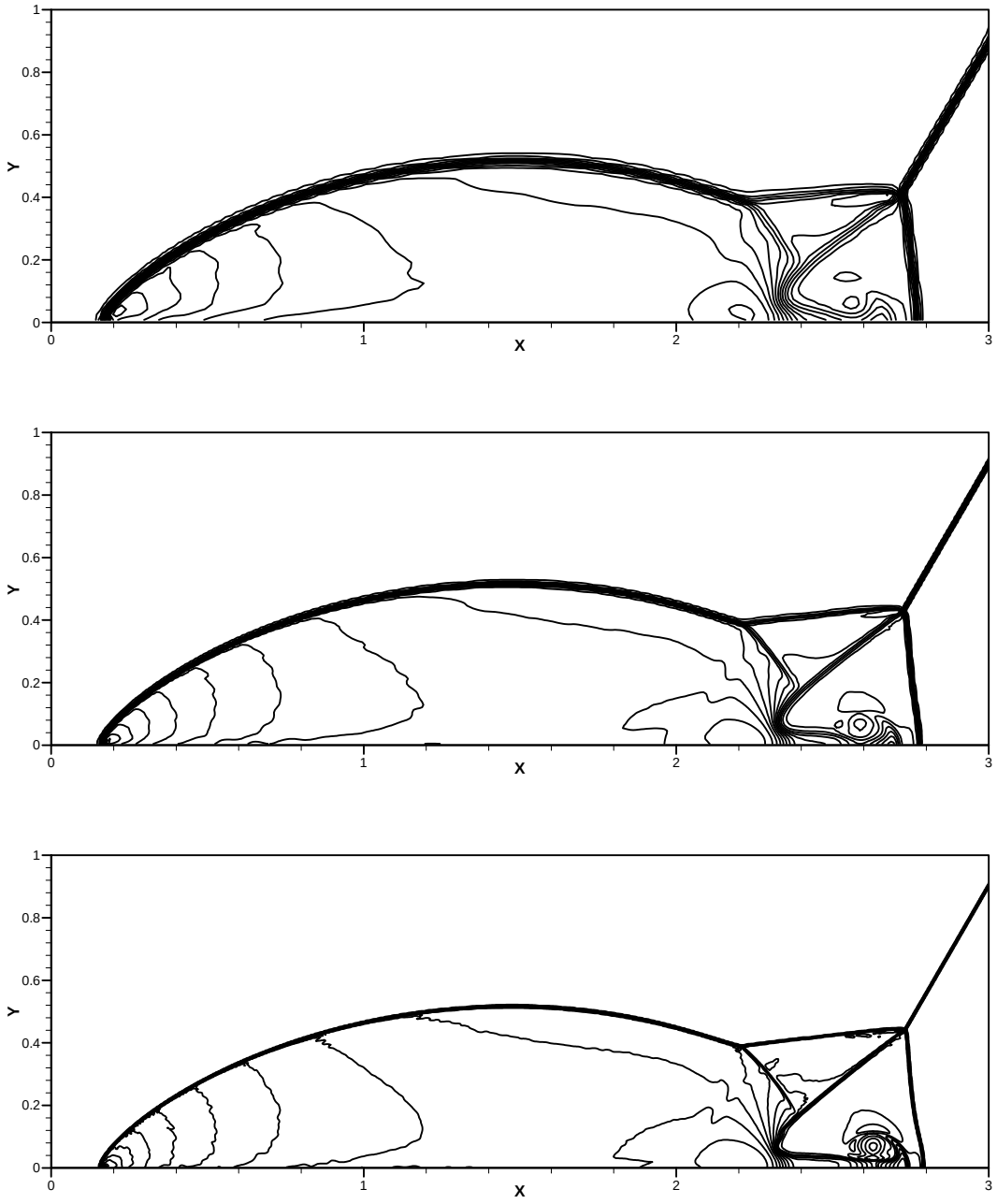

Figure 16: Double Mach reflection problem for the WENO-MUSTA$_2$-3 flux. Meshes of 240×60 (top), 480×120 (middle) and 960×240 (top) cells are used. 30 contour lines from 2 to 22.

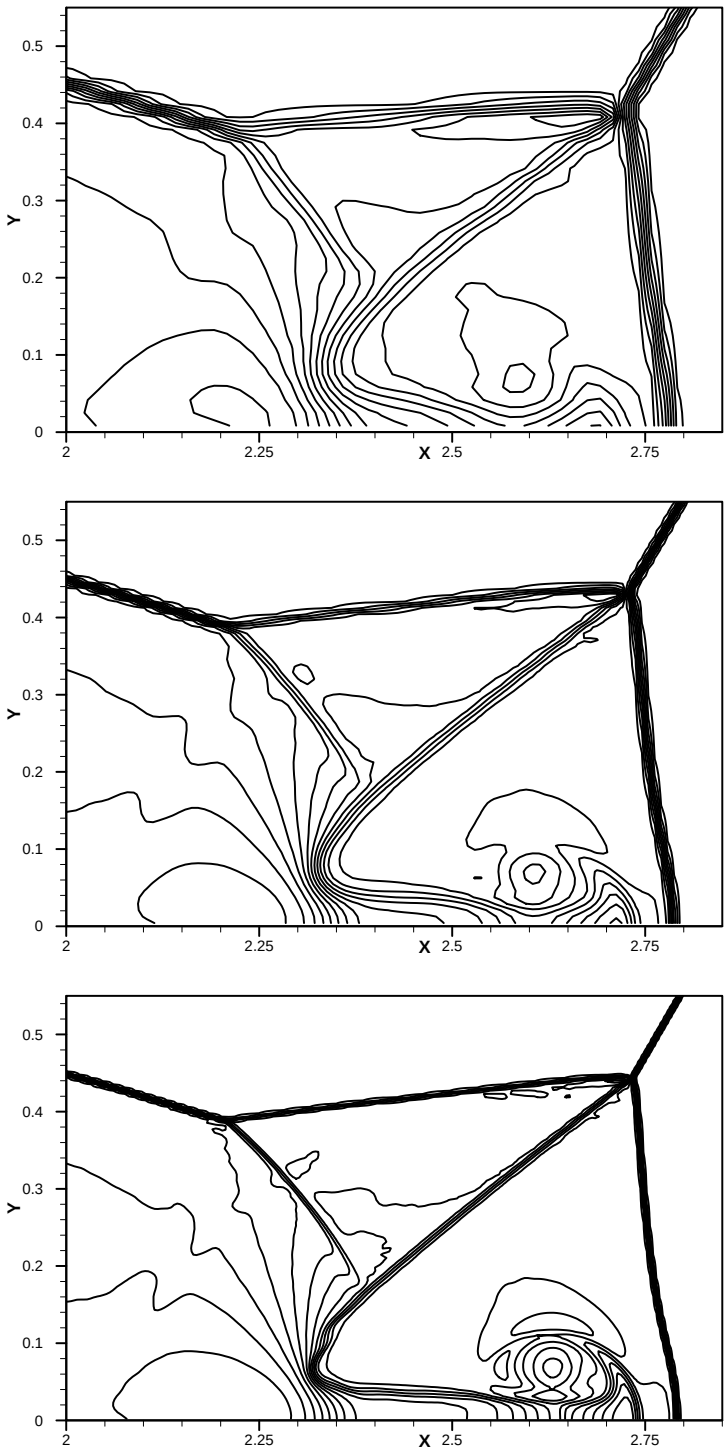

Figure 17: Double Mach reflection problem for the WENO-MUSTA$_2$-3 flux. Zoom of the blow-up region of Fig. 16

7.2.2 Double Mach reflection of a strong shock [21]

We solve the two-dimensional Euler equations in a rectangular domain. The formulation of the problem, computational setup and detailed discussion of the flow physics can be found in [21]. At the given output time a complicated flow pattern forms containing two Mach shocks, two slip surfaces and a jet. Figs. 16–17 show numerical results of the WENO scheme with the new MUSTA$_2$-3 flux on three meshes: 240×60, 480×120 and 960×240 cells. We observe that the schemes produce the flow pattern generally accepted in the present literature [21, 11] as correct, on both meshes. All discontinuities are well resolved and correctly positioned.

The delicate features of the flow, such as slip surfaces, are more difficult to resolve accurately. For these the results of the present scheme are more accurate than those of the original scheme (6), found in Figs. 3, 5 of [12] and comparable to those of the scheme with the state-of-the art HLLC flux [19] found in Figs. 2, 4 of [12].

We have also run the spatially seventh order version of the scheme, with good results. The corresponding plots are omitted.

8 Conclusions

In this paper we developed an improved version of the Multi-Stage (MUSTA) approach to the construction of upwind Godunov-type fluxes. An analysis of the original MUSTA and new MUSTA of the present paper shows that the new schemes improve upon the original ones in terms of monotonicity properties, accuracy and stability in multiple space dimensions. In particular, for the linear advection equation with constant coefficients stability region of new MUSTA schemes coincides with that of the Godunov method and the truncation error converges to that of the Godunov method as the number of stages grows. For non-linear systems the more economical one-stage MUSTA$_2$-1 scheme has accuracy close to that of the Godunov method with the exact Riemann solver in one space dimension and the three-stage MUSTA$_2$-3 scheme is effectively as accurate as the Godunov scheme in most cases.

The main advantage of schemes with MUSTA fluxes over centred schemes lies in much better accuracy and stability. Therefore, our new schemes are good alternatives to current centred methods and to conventional upwind methods as applied to complicated hyperbolic systems for which the solution of the Riemann problem is costly or unknown.

Acknowledgments. Part of the paper was finalized during the stay of the first author at the Isaac Newton Institute for Mathematical Sciences, University of Cambridge

and participation in the programme *Nonlinear Hyperbolic Waves in Phase Dynamics and Astrophysics*. The second author acknowledges the support provided by the Isaac Newton Institute for Mathematical Sciences, University of Cambridge, UK, as co-organizer of the six-month programme on *Nonlinear Hyperbolic Waves in Phase Dynamics and Astrophysics*, January to July 2003, and the associated EPSRC senior visiting fellowship, grant No GR N09276.

References

[1] G. Q. Chen and E. F. Toro. Centred schemes for nonlinear hyperbolic equations. *J. of Hyperbolic Differential Equations*, 1(3):531–566, 2004.

[2] P. Colella. Multidimensional upwind methods for hyperbolic conservation laws. *J. Comput. Phys.*, 87:171–200, 1990.

[3] S.K. Godunov. A finite difference method for the computation of discontinuous solutions of the equations of fluid dynamics. *Mat. Sbornik*, 47:357–393, 1959.

[4] A. Harten, P. D. Lax, and B. van Leer. On upstream differencing and Godunov-type schemes for hyperbolic conservation laws. *SIAM Review*, 25(1):35–61, 1983.

[5] V.P. Kolgan. Application of the minimum-derivative principle in the construction of finite-difference schemes for numerical analysis of discontinuous solutions in gas dynamics. *Uch. Zap. TsaGI*, 3(6):68–77, 1972. in Russian.

[6] V.P. Kolgan. Finite-difference schemes for computation of three dimensional solutions of gas dynamics and calculation of a flow over a body under an angle of attack. *Uch. Zap. TsaGI*, 6(2):1–6, 1975. in Russian.

[7] A. G. Kulikovskii, N. V. Pogorelov, and A. Yu. Semenov. *Mathematical Aspects of Numerical Solution of Hyperbolic Systems*. Chapman and Hall, 2002. Monographs and Surveys in Pure and Applied Mathematics, Vol. 118.

[8] P.D. Lax. Weak solutions of nonlinear hyperbolic equations and their numerical computation. *Comm. Pure Appl. Math.*, 7:159–193, 1954.

[9] P.D. Lax and B. Wendroff. Systems of conservation laws. *Comm. Pure Appl. Math.*, 13:217–237, 1960.

[10] D. Levy, G. Puppo, and G. Russo. A fourth order central WENO scheme for multi-dimensional hyperbolic systems of conservation laws. *SIAM J. Sci. Comput.*, 24:480–506, 2002.

[11] J. Shi, C. Hu, and C.-W. Shu. A technique for treating negative weights in WENO schemes. *J. Comput. Phys.*, 175:108–127, 2002.

[12] V.A. Titarev and E.F. Toro. Finite-volume WENO schemes for three-dimensional conservation laws. *J. Comput. Phys.*, 201(1):238–260, 2004.

[13] E.F. Toro. On Glimm-related schemes for conservation laws. *Technical Report MMU-9602, Department of Mathematics and Physics, Manchester Metropolitan University, UK.*, 1996.

[14] E.F. Toro. *Riemann Solvers and Numerical Methods for Fluid Dynamics.* Springer-Verlag, 1999. Second Edition.

[15] E.F Toro. Multi-stage predictor-corrector fluxes for hyperbolic equations. *Preprint NI03037-NPA. Isaac Newton Institute for Mathematical Sciences, University of Cambridge, UK*, 2003.

[16] E.F Toro. MUSTA: A multi-stage numerical flux. *Preprint NI04008-NPA. Isaac Newton Institute for Mathematical Sciences, University of Cambridge, UK*, 2004.

[17] E.F. Toro and S.J. Billett. Centred TVD schemes for hyperbolic conservation laws. *IMA J. Numerical Analysis*, 20(1), 2000.

[18] E.F. Toro and W. Hu. Centred Unsplit Finite Volume Schemes for Hyperbolic Conservation Laws. In E.F. Toro, editor, *Godunov Methods: Theory and Applications*, pages 897–902. Kluwer Academic/Plenum Publishers, 2001.

[19] E.F. Toro, M. Spruce, and W. Speares. Restoration of the Contact Surface in the Harten-Lax-van Leer Riemann Solver. *Journal of Shock Waves*, 4:25–34, 1994.

[20] B. van Leer. Towards the ultimate conservative difference scheme V: a second order sequel to Godunov' method. *J. Comput. Phys.*, 32:101–136, 1979.

[21] P. Woodward and P. Colella. The numerical simulation of two-dimensional fluid flow with strong shocks. *J. Comput. Phys.*, 54:115–173, 1984.